RSC Advances

PAPER

View Article Online
View Journal | View Issue

Cite this: *RSC Adv.*, 2022, **12**, 2074

Enrichment of gas storage in clathrate hydrates by optimizing the molar liquid water–gas ratio

Sai Kiran Burla [ab] and S. R. Prasad Pinnelli *[ab]

Natural gas (NG) is considered a modern source of energy. Gas hydrates are anticipated to be an alternative method for gas storage and transportation applications. The process must be handy, rapid, and proficient for scale-up. In the present study, methane (CH_4) and carbon dioxide (CO_2) hydrates are synthesized by varying the guest (gas) to host (water) volume. The experiments are performed in a non-stirred system. The results specify that the maximum storage capacity is achieved when the molar liquid water–gas ratio is about 4.08 and 8.25 for CH_4 and CO_2 hydrates. At the optimal water–gas ratios, the total CH_4 and CO_2 gas uptake capacity is about 14.3 ± 0.4 and 9.1 ± 0.4 liters at standard temperature and pressure (STP) conditions. The gas uptake gradually increases with the solution volume and abruptly falls after a threshold point. The hydrate grows across the reactor's metal surface; when the process fully covers the surface, the growth continues horizontally (increase in thickness). With varying the liquid water–gas ratio (low to high), the formation kinetics (t_{90}) is delayed. The hydrate growth rate gradually decreases and does not significantly influence the hydrate formation temperatures. Optimizing the molar liquid water–gas ratio yields a high gas storage capacity and faster process kinetics.

Received 13th October 2021
Accepted 24th December 2021

DOI: 10.1039/d1ra07585c

rsc.li/rsc-advances

1. Introduction

1.1. Gas hydrates

Clathrate hydrates, also called gas hydrates, are ice-like crystalline compounds. The gas molecules are trapped in the water molecules' cavities developed by hydrogen bonding under suitable temperature and pressure conditions.[1] A weak van der Waals interaction confines the motion of the gas molecules within the hydrate structure. Based on the size, shape, and nature of the gas molecules, the hydrate structures are classified into three types, namely structure I (sI), structure II (sII), and structure H (sH). In nature, these hydrates form naturally in the permafrost and ocean depths.[2–7] The natural hydrates mainly comprise methane gas.[8] Natural hydrates are ascertained to be a future energy source if used with feasible technology and will have economic value.[9] The synthetic hydrates provide multi-faceted applications such as storage media for greenhouse gases,[10–16] carbon dioxide capture from fuel gas,[17] methane recovery from coal mine gas,[18,19] desalination,[20–22] cold storage,[23–27] and gas transportation.[12,28] Because of their structural properties and selectivity, this process slowly escalates to address various food technology issues.[29] On one side, they serve as a technological solution for modern-day problems; conversely, these hydrates are considered a bottleneck in the oil and gas industry.[30] The hydrate plug formation in pipelines during production and transportation is hazardous. Several researchers have addressed possible solutions to minimize these issues.[31–39]

1.2. Conventional methods for gas storage & transportation

With the increasing population, the demand for energy consumption is high. Natural gas (NG) is the cleanest burning fossil fuel, contributing 24.2% of the world's total primary energy consumption.[40] Being the pristine and less CO_2 emitter, the natural gas demand is expected to be increasing in the coming years. The conventional gas storage and transportation methods are through compression (CNG) and liquefaction (LNG).[41,42] Although the commercial development is *via* CNG and LNG, their complications are risky and unsafe. In CNG, the gas is stored by compressing it to less than 1% volume at standard temperature & pressure (STP) conditions. As a result, the gas is stored in high-pressure conditions. This leads to the high-pressure cylinder requirement (20–25 MPa). The CNG process requires huge compressors to compress the gas to 20–25 MPa, and the energy needed by these engines is high, which consumes high electricity. The process takes a long time and is noisy, sometimes requires multistage, and the overall budget to maintain and operate these plants is expensive. Also, the transport containers are designed heavy-walled (adds weight to the transport vehicle). The effect of tank weight on the mileage and payload is a hindering factor. Fluctuations/increases in the ambient temperatures could influence or limit the storage capacity in CNG tanks. The transportation of the gas to long

[a]*Gas Hydrate Division, CSIR-National Geophysical Research Institute (CSIR-NGRI), Hyderabad-500 007, India. E-mail: psrprasad@ngri.res.in; Fax: +91 40 2717 1564; Tel: +91 40 2701 2710*

[b]*Academy of Scientific and Innovative Research (AcSIR), Ghaziabad-201002, India*

distances and changes in the ambient temperature with locations could trigger the expansion of gas and is unsafe.[42] In LNG, the gas is condensed into a liquid by compressing it to 1/600 times volume at STP. The gas exists in liquid form at atmospheric pressure and low-temperature conditions (−162 °C). For the transportation of LNG, special cryogenic containers are required, which in turn requires high investment.[41] In comparison with CNG and LNG, LNG is most preferred for the long-distance transport of natural gas because of its high volumetric capacity. Studies show the economic feasibility of gas hydrates, *i.e.*, the hydrating process's overall cost is much lower than that of the LNG process.[43] Another primary concern associated with the LNG procedure is the emission of industrial pollutants such as CO_2 and SO_2 during the production process. The LNG process consists of four operational stages wherein stage (i) upstream gas production (feed gas), (ii) pre-treatment, (iii) liquefaction, and (iv) shipping and regasification. The natural gas supplied from the source point is refined, and impurities such as CO_2, CO, SO_2, and H_2S are vented out in the pre-treatment process through various separation methods. These pollutant gases discharged during the liquefaction process must be properly treated, reprocessed, and reused, to reduce environmental pollution.[44,45] Different methodologies are adopted to facilitate the process cost, and search for an alternative medium is in demand.[46] Also, studies report that 70% of the gas reserves are far or small to connect with the existing pipeline connections or liquefaction facility.[47]

1.3. Hydrate technology for gas storage & transportation

Hydrate-based technology is preferred and could potentially bypass the above-mentioned technical issues and effectively explore the gas resource.[48,49] Gas hydrates can compress a large gas volume in a small space and act as a potential gas storage medium. Ideally, the unit volume of gas hydrate would give 160–180 times of gas upon dissociation.[1,30] Also, the moderate formation conditions and minimum energy requirement for complete recovery of the stored gas are advantageous.[50] The storage and transportation of gas *via* hydrate technology are in demand because of their high safety. Comparatively 18–24% lower cost than LNG transportation.[43,51] Though hydrate-based technology offers economical and feasible solutions over CNG and LNG, few bottlenecks are associated with this process. The inefficient water-to-hydrate conversion and the sluggish kinetics are primary concerns to scale up this process.[1] Several researchers over the past decades established and proposed various methods to overcome these bottlenecks. Mechanical techniques such as stirring the sample solution, spraying the liquid, and continuously injecting gas into the liquid phase enhance the gas water interaction.[52] Thermodynamic promoters such as tetrahydrofuran, cyclopentane, tetra-*n*-butyl ammonium bromide, and epoxycyclopentane increase the hydrate stability conditions to higher temperatures.[11,53–60] The use of packed beds, porous materials, nanoparticles, dry water, foams, and hydrogels proved to accelerate the growth kinetics and higher gas uptake by increasing the surface area.[10,61–66] Surfactants such as sodium dodecyl sulfate, sodium benzenesulfonate, alkyl benzene sulfonates, *etc.*, are studied rigorously. Studies report that the micelle formation and the decreased surface tension offer higher gas water interaction and enhance mass transfer.[67–71] All these methods and materials are good at laboratory scale, but industrial-scale may hamper the cost and technical constraints. Recently additives such as amino acids and bio powders are proved to be kinetic hydrate promoters for CH_4 and CO_2 hydrates.[12,13,72–75] The hydrates are formed easily at moderate temperature and pressure conditions. No additional stirring or mixing is required. Also, 90% of the hydrate conversion is in less than an hour. Thus, using these water-soluble additives could better serve faster kinetics, higher hydrate yield, and ease to pelletize for storage and transportation application.

The present study explains the formation of methane and carbon dioxide hydrates in the presence of low dose (0.5 wt%) L-methionine amino acid (L-met). L-Methionine is a kinetic hydrate promoter for both CH_4 and CO_2 hydrates.[12,72,75] Emphasis is to achieve rapid kinetics, higher uptake capacity, and exhibit a simple experimental setup to reduce the overall process cost. An attempt is made to understand the role of reactant concentrations in maximizing the process yield. The experiments are performed by varying the solution bed height and free gas. The process operation is simple since the amino acid is easily soluble in water, and the formation conditions are moderate. The reactor design does not require additional stirring, which could be a worthy setup if escalated to real-time use.

2. Experimental section

2.1. Materials

99.95% purity methane and carbon dioxide gases are used to perform experiments procured from M/S Bhuruka Gas Company. Deionized water type 1 is used to make the sample solution. The amino acid powder is purchased from M/S Sigma Aldrich and is used as received.

2.2. Apparatus

The apparatus includes a high-pressure reactor vessel (500 ml volume) made of SS-316 and can hold up the pressure to 10 MPa. The temperature is controlled by a closed-loop chiller (ANCRYO-LTCCB-40) with a circulating liquid tank attached to it. Glycol and water mixture in the selected ratio is used as a coolant. The temperature and pressure measurements are recorded using platinum resistance thermometers (Pt100) and a pressure transducer (WIKA, type A-10 for pressure range 0–25 MPa with ±0.5% accuracy).

2.3. Procedure

The experiments are performed in a batch reactor following the isochoric method procedure. The aqueous sample solution of the chosen volume is poured into the reactor vessel. The sample gas with desired pressure is filled into the reactor vessel through the inlet valve using the Teledyne ISCO syringe pump. Before introducing the gas, the reactor cell is purged with sample gas 3–4 times. The pump is disconnected after introducing the gas.

The reactor vessels are immersed into the coolant tank. The chiller is set to the desired experimental value to increase or decrease the reactor vessel's temperature. The hydrate formation is inferred from the temperature spike because of the exothermic heat release during the hydrate crystal growth. The gas consumed in the hydrate conversion process is calculated from the observed pressure drop. Subcooling is the difference between the phase equilibrium temperature at the operating pressure and the experimental formation temperature. Each experiment is repeated at least three times, and the data is represented with an average value and standard deviation. The schematic experimental design is shown in Fig. 1. The temperature and pressure data points are recorded every 30 seconds. In all the cycles, the experimental parameters were kept constant.

2.4. Equations used for data calculations

The following equation defines the molar gas concentration of CH_4 and CO_2 gas in the hydrate phase during an experiment at any given time t.

$$\Delta n_{H,t} = n_{g,0} - n_{g,t} = \left[\frac{P_0 V}{Z_0 R T_0}\right] - \left[\frac{P_t V}{Z_t R T_t}\right] \quad (1)$$

where, Z – is the compressibility factor, calculated using the Peng–Robinson equation of state. P – pressure, V – volume, T – temperature, R – gas constant 0 – initial point, t – a point at any given time.

The volume changes during phase transformation are neglected, and volume is constant throughout the experiment.

The gas consumption rate was computed using forward differentiation by the following equation.

$$\text{Gas uptake rate} = (n_{i+\Delta t} - n_i)/\Delta_t \quad (2)$$

where Δt is fixed time interval and n_i is the content of gas at the i^{th} minute.

The amount or percentage of water converted into hydrate is calculated using the following equation.

$$\text{Hydrate conversion} = \frac{\Delta n_H \times \text{hydration number}}{n_{H_2O}} \times 100 \quad (3)$$

where Δn_H are the total moles of gas consumed in the hydrate formation process and n_{H_2O} is the total number of moles of water used in the process.

The following equation calculates the hydration number

$$\text{For structure I: } 46/(2(\theta_s) + 6(\theta_l)) \quad (4)$$

where 46 are water molecules for sI hydrates and θ_s and θ_l are the small and large cage occupancy of gas molecules calculated using CSM GEM application. [1]

The following equation defines the molar liquid water–gas ratio.

$$\Phi = V_w/V_g \quad (5)$$

where Φ is the molar liquid water–gas ratio, V_w is the volume of water (mole) added to the reactor, and V_g is the volume of gas (mole).

The conversion of consumed gas (mole) into liters is by the following equation

$$V = \frac{(\Delta n_H \times M)}{\rho} \Big/ 1000 \quad (6)$$

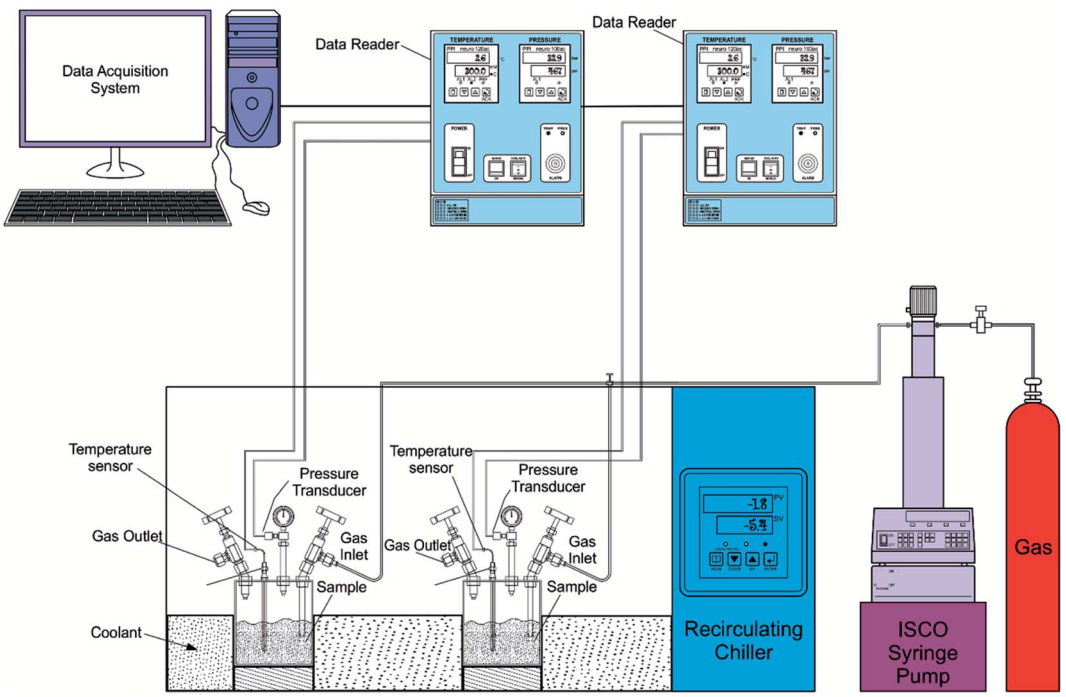

Fig. 1 The schematic experimental design of the hydrate formation process.

where V is the volume of gas (liters), Δn_H is the of gas consumed (mole) in hydrate phase, M is the molar mass (g mol^{-1}) of the gas and ρ is the density (g cm^{-3}) of the gas.

3. Results and discussion

3.1. CH_4 and CO_2 hydrate formation conditions

Methane, a principal constituent, and carbon dioxide, a secondary component of natural gas, are of primary concern for climate change. Gas hydrates are considered the best materials for gas storage and transportation applications with high storage capacity. The CH_4 and CO_2 hydrates are synthesized by varying the molar liquid–gas volume in the isochoric method. 0.5 wt% of the L-methionine (L-met) is added to water to accelerate the reaction process. In the presence of amino acids, the hydrate growth is rapid.[12] The reusability of the sample is easy and yields the exact conversion. It is non-foaming and is feasible for pelletizing. The complexity with experimental design increases when scaling to higher capacities. Since stirring/mixing or spraying the liquid becomes difficult and adds additional cost, we performed the experiments in a non-stirred condition. The formation and dissociation of the CH_4 and CO_2 hydrates are at moderate pressure-temperature conditions. The experiments are performed with 30, 60, 90, 200, and 330 ml of varying sample volumes. Fig. 2 shows the CH_4 and CO_2 hydrates' pressure-temperature trajectory synthesized with 90 ml of the sample solution.

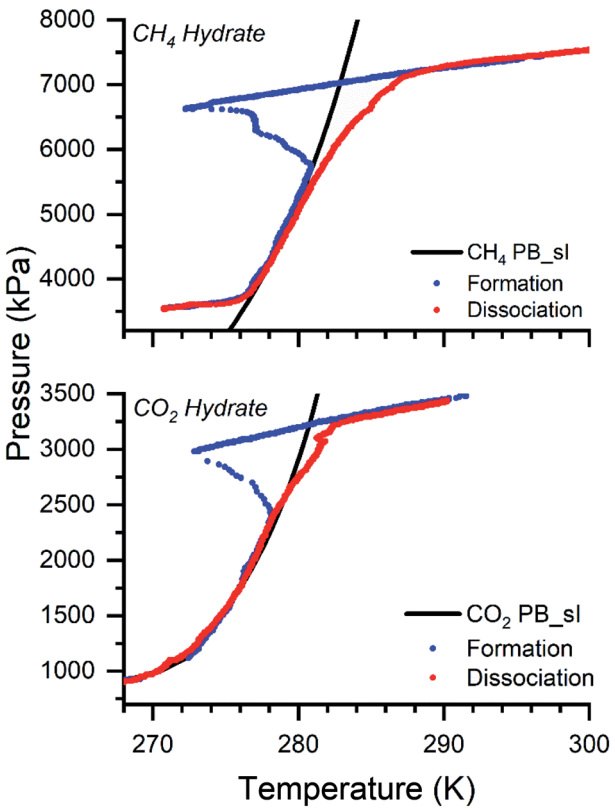

Fig. 2 The graph shows the formation and dissociation of the CH_4 and CO_2 hydrates with a 90 ml volume solution. The black line represents the theoretical phase boundary curve for CH_4 and CO_2 hydrates, computed from CSM GEM application.[1] The blue and red dots show the formation and dissociation cycles for both gases.

The black line represents the theoretical phase equilibrium boundary for CH_4 and CO_2 hydrates generated using the CSM GEM application.[1] The blue and red dots show the hydrate formation and dissociation pattern. The initial experimental conditions are 7500 and 3500 kPa at ambient temperature 298 K for CH_4 and CO_2 systems. The operating conditions are chosen since a higher driving force offers a faster reaction rate and enhances the yield.[11,72,74] The gas is introduced at 298 K. As the reactor temperature decreases, the gas linearly decreases. Once the phase equilibrium boundary is crossed, a steep reduction in the pressure is observed. A sharp increase in the temperature with an abrupt decrease in pressure is observed at one point. This point is termed the nucleation point, which indicates the hydrate nucleation (exothermic reaction). With time, the pressure reduction reaches saturation, and a linear behavior is observed with a further decrease in temperature. This point defines the saturation of the hydrate growth and confirms the end of the reaction. Further heating up the system, the hydrate dissociates, and the captured gas in the hydrate cages is released. The hydrate dissociation (red dots) is governed and followed along the phase equilibrium curve. To observe the dissociation pattern, the warming is performed at 0.5–1 K/H (ideally, it could be performed at a faster heating rate to degasify). At higher pressures, the deviation on the dissociation is due to the faster heating rate. The experiments are repeated three times at each sample volume, and the average value is taken for presentation. The formation temperature and pressure conditions are not varied with the sample volumes. They are in the range 270–272 K and 6600–6800 kPa for CH_4 hydrates and 272–273 K and 2600–2900 kPa for CO_2 hydrates. At 90 ml sample volume, the formation temperature and pressure points for CH_4 hydrate are around 271.6 $\pm$ 0.8 K and 6610 $\pm$ 28.3 kPa, and for the CO_2 system is around 273 $\pm$ 0.9 K and 2800 $\pm$ 20 kPa. In all the experiments, it is ensured the driving force is constant. Driving force is defined as the difference between the experimental and the equilibrium pressure (calculated from CSM GEM).[1].

3.2. Optimizing the molar liquid water–gas ratio

Fig. 3 shows the gas uptake into the hydrates with varying volumes.

The graph shows the amount of gas consumed (in liters at STP conditions) in the hydrates with varying solution capacities. The red and black dots represent the CH_4 and CO_2 hydrate storage capacities. The maximum gas consumed by the hydrates is around 90 ml in both systems. An abrupt decrease in the gas uptake is seen around 200 ml for the CO_2 system; hereafter, we did not perform experiments with the further increasing solution concentration. The gas intake into the hydrates is linearly increased until the solution volume is 90 ml. Another addition to the solution, the gas intake capacity abruptly decreased. This reduction signifies the importance of the reactant's volume in

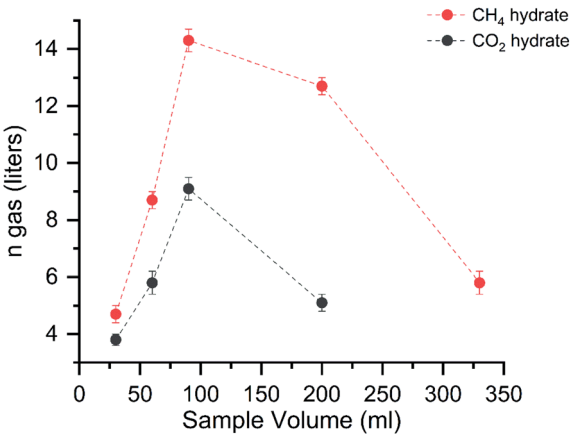

Fig. 3 The graph shows the gas uptake capacity (liters at STP conditions) with varying sample volumes. The red and black dots correspond to the average value of CH_4 and CO_2 hydrate systems with standard deviations.

the hydrate conversion. It is defined as a molar liquid water–gas ratio, a dimensionless quantity represented by eqn (5).

The gas uptake capacity is in increasing trend up to 90 ml solution. At a lesser sample volume, the availability of free gas molecules is high. The overall hydrate yield in 30, 60, and 90 ml is about ~80% for methane hydrates and ~60% for carbon dioxide hydrates (see Table 1). This means the maximum water is utilized in the hydrate conversion process. At 30 and 60 ml, the absolute gas molecules captured into the hydrates are less than 90 ml solution showing the available space for gas encasing is fewer due to the lesser availability of the water molecules. Further increase in the solution quantity, the free space for the available gas molecules is less, and the hydrate growth is limited. The gas uptake kinetics for the CH_4 and CO_2 systems with different water–gas ratios are shown in Fig. 4.

Fig. 4 shows the plot, reaction time *vs.* gas uptake capacity for the methane (a) and carbon dioxide (b) hydrates with varying molar liquid water–gas ratios. The absolute gas uptake is significantly less with increasing the solution's quantity. When the molar liquid water–gas ratio is 1.16 and 2.35, the storage capacity and the reaction time (t_{90} – the time required for completing 90% of the reaction process) is about 4.7 ± 0.2, 3.8 ± 0.2 liters, and 9.5 ± 1.4, 34.3 ± 7.7 minutes for CH_4 and CO_2 systems. When the ratio increases to 2.5 and 5.07, the storage capacity is double, and the reaction time increases 2 and 3 times for CH_4 and CO_2 systems. The maximum storage capacity is obtained when the water–gas ratio is 4.08 and 8.25 for CH_4 and CO_2 hydrates. The total CH_4 and CO_2 gas uptake are about 14.3 ± 0.4 and 9.1 ± 0.4 liters (at STP conditions), further increasing the ratio to 13.18 (CH_4) and 26.66 (CO_2), the gas storage capacity abruptly decreases. The average data points of formation temperature, pressure, and the amount of hydrate conversion at each bed height for both CH_4 and CO_2 system and the subcooling required, formation kinetics, the gas uptake rate, and the molar liquid water–gas ratio of the reactor are tabulated in Table 1. Close observation shows the t_{90} kinetics for the two gas systems vary with increasing the solution concentration—the lesser the solution volume, the faster the hydrate growth kinetics. The t_{90} for 30, 60, 90, 200, and 330 ml solution quantity is 9.5, 26.5, 61.5, 132, and 109 minutes for CH_4 and is about 34.3, 89, 144.8, and 153 minutes for the CO_2 system. With an increase in the solution quantity, the time required for 90% of the hydrate formation increased 10 and 4 times higher for CH_4 and CO_2 systems. From Fig. 4, it is apparent that the molar liquid water–gas ratio has a strong influence on the hydrate formation process. The reaction time is faster at a lower ratio and has considerable uptake capacity. The uptake capacity is high at a higher ratio (optimal condition) but longer reaction time. The appropriate or optimal water–gas ratio used in this work is 4.08 and 8.25 for CH_4 and CO_2 systems.[76] The hydrate conversion is maximum when the reactant volume is 20–25% of the total reactor volume.

Similarly, Rossi *et al.* developed a high-pressure spray reactor with a 25 liter capacity to enhance methane uptake.[77] The liquid is sprayed into the reactor filled with gas. The maximum gas uptake is achieved when the sample volume is about 5 liters,

Table 1 The table shows the average data points of formation temperature, pressure, and the amount of hydrate conversion at each bed height for both CH_4 and CO_2 systems. The subcooling required, formation kinetics, the gas uptake rate, and the molar liquid water–gas ratio of the reactor are tabulated

S. no.	Sample volume (ml)	$T_{formation}$ (K)	$P_{formation}$ (kPa)	Hydrate yield (%)	Gas consumed (liters at STP)	Subcooling (K)	t_{90} kinetics (min)	Gas uptake rate (mmol min^{-1})	Molar liquid water–gas ratio (Φ)
CH_4 hydrate									
1	30	270.9 ± 0.9	6635 ± 148.5	78.1 ± 3.6	4.7 ± 0.2	11.8 ± 0.6	9.5 ± 1.4	23.4 ± 0.9	1.16
2	60	270.7 ± 0.8	6630 ± 56.6	72.9 ± 3.1	8.7 ± 0.5	12.3 ± 0.7	26.5 ± 7.8	18.6 ± 1.1	2.5
3	90	271.6 ± 0.8	6610 ± 28.3	81 ± 2.8	14.3 ± 0.4	11.2 ± 0.9	61.5 ± 6.3	13.1 ± 0.6	4.08
4	200	270.3 ± 2.5	6520 ± 56.6	32.2 ± 1.5	12.7 ± 0.3	12.5 ± 2.6	132 ± 8.4	6.8 ± 0.3	13.18
5	330	270.4 ± 0.9	6730 ± 14.1	8.9 ± 1.8	5.8 ± 0.3	13 ± 0.8	109 ± 4.9	7.4 ± 0.3	46.76
CO_2 hydrate									
1	30	273.2 ± 2.5	2973.3 ± 110.1	71.1 ± 1.4	3.8 ± 0.2	7.5 ± 2.3	34.3 ± 7.7	5 ± 0.2	2.35
2	60	272.1 ± 1.1	2760 ± 42.4	52.8 ± 3	5.8 ± 0.4	8.3 ± 1.1	89 ± 8	4.8 ± 0.3	5.07
3	90	273 ± 0.9	2800 ± 20	56.1 ± 3.1	9.1 ± 0.4	7.2 ± 1	144.8 ± 51.3	3.1 ± 0.1	8.25
4	200	273.3 ± 2.3	2600 ± 127.3	14 ± 1.2	5.1 ± 0.3	6.8 ± 2.5	153 ± 63.6	2.6 ± 0.2	26.66

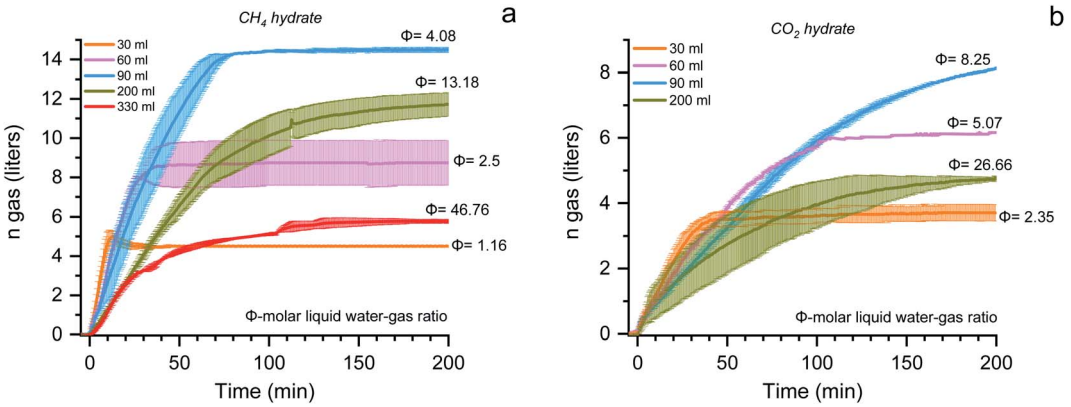

Fig. 4 The gas uptake (in liters at STP conditions) kinetics for the methane (a) and carbon dioxide (b) hydrates formed with different molar liquid water–gas ratios is represented. The colored line represents the average value, and the shaded portion represents the standard deviation from repetitive measurements.

corresponding to 20% of the total reactor volume. The study also reported that the hydrate growth is mainly on the metal surfaces of the reactor. Pang *et al.* studied the scale-up effect for gas storage in the form of hydrate in a quiescent reactor (10 liters capacity).[78] Methane hydrate was synthesized using sodium dodecyl sulfate as an additive. They assessed the various parameters in scaling the hydrating process, such as water quantity's impact on the storage capacity, formation rate, the effect of the double-deck cells, deck height and plate span, and liquid water's role. The study reported that the gas uptake capacity and the hydrate formation rate decreased with the increased sample solution quantity. The morphological observation revealed that the hydrate growth is dominantly on the metal surfaces of the reactor. A multi-deck cell type vessel is used as an internal part of the reactor to enhance the growth rate, where the hydrates form inside the cells. The volume of each cell and the quantity of water loaded do not alter the specific formation rate. The liquid's role is assed to show the tap water could be used instead of the expensive distilled water. Our observations strongly agree with the earlier experimental results. The gas uptake capacity decreased by 60 and 40% when the sample volume was increased to 330 and 200 ml for CH_4 and CO_2 hydrates. When the quantity of water is less (30 and 60 ml), the gas uptake capacity is high. The decrease in the storage capacity speeded up when the water quantity exceeded 90 ml for both systems.

3.3. Hydrate growth morphology

It is observed the hydrate formation is mainly on the surface of the reactor. This creep behavior ensures enhanced interaction between water molecules *via* capillary action and gas molecules, thus promoting rapid and efficient hydrate conversion.[12,78] Fig. 5 shows the hydrate formation *via* creep behavior on the metal surface of the reactor.

The hydrate saturation is ensured, the reactor temperature is lowered to 150 K, and simultaneously depressurized. The head part is removed from the reactor, and the photograph is captured. At the gas–water interface, the hydrate particle triggered moves upward rapidly to adsorbed on the metal surface. The water level is decreased as the hydrate grows across the reactor walls. This is because of the water creep phenomenon *via* capillary pores. This leads to a remarkable increase in the gas–water interface and results in rapid and higher gas uptake. The hydrate grows upwards, above the liquid level along the reactor's metal surface; when all the metal surface is covered with hydrate creep, the hydrate increases in thickness (see circled portions in Fig. 5). During this process, the water adsorbed by the hydrate particles became interstitial, which does not directly contact the gas. The gas water interaction is possible only through the diffusion process, a controlling factor for hydrate growth. Since the hydrate's conductivity is low, the heat transfer would become another control step where the hydrate growth would decrease dramatically with increasing thickness.[78] This is evident from Fig. 5, where the hydrate thickness is large once it reaches the top of the reactor wall and is small when the hydrate growth is at the bottom (see circled portions in Fig. 5). The hydrate could easily creep along the reactor wall when the sample quantity is less. The gas water interaction is enhanced, heat transfer is easy, and the hydrate growth kinetic is faster. With increased sample quantity, the reactor's bed height increases, reducing the metal surface area for hydrate to creep. It starts to grow in thickness, hindering the gas water interaction. Heat transfer delays the further hydrate growth. The rate calculation for CH_4 and CO_2 systems is shown in Fig. 6.

Initially, at 30 ml of the solution, the gas uptake rate is high, about 23.4 and 5 mmol min^{-1} for CH_4 and CO_2 systems. As the sample solution increases, the gas uptake rate tends to decrease. As said earlier, when the surface area is high and hydrate rapidly grows across the walls, which yields a higher gas uptake rate. The walls' surface areas are reduced with increased solution volume, and the hydrate grows in thickness. The diffusion process controls the interaction of gas water, and the heat transfer is limited, resulting in sluggish hydrate growth and a slower gas uptake rate. Similar studies on the surface area to volume optimization for sII hydrates with varying volumes of

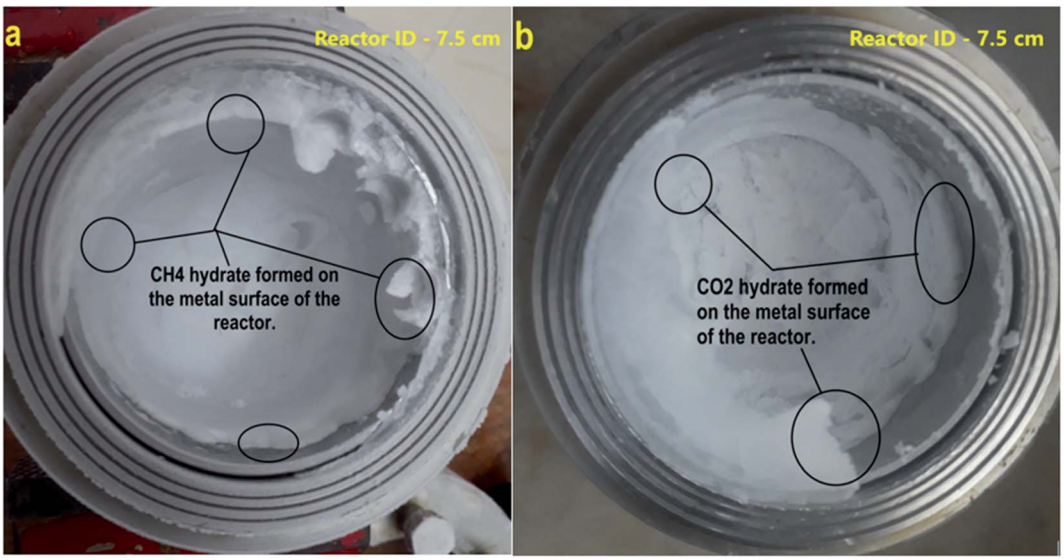

Fig. 5 The image shows the hydrate growth morphology for (a) CH_4 hydrate (b) CO_2 hydrate (hydrates formed inside the reactor with internal diameter (ID) of 7.5 cm, the image captured from the top side). The circled parts show the sample at the start of the hydrate creeping (bottom position) and the hydrate growing horizontally (top position).

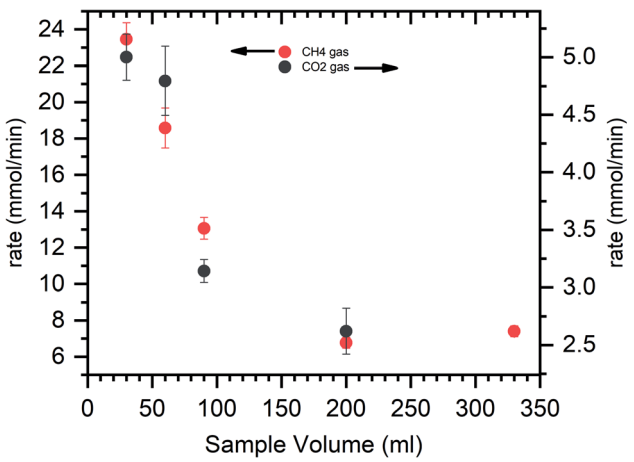

Fig. 6 The plot represents the gas uptake rate *vs.* sample volume for methane and carbon dioxide hydrates. The red dots indicate the CH_4 system, and the black dots indicate the CO_2 system. The average value is shown with a standard deviation from repetitive measurements.

tetrahydrofuran + CH_4 are studied by Kiran *et al.* and Veluswamy *et al.*[11,79,80] The results reported the maximum gas consumption has occurred at half the reactor volume. The hydrate grows with a distinct hollow crater-like formation aided by well-connected channels for liquid flow upward along the reactor walls and simultaneous dendritic crystal growth within the solution in a downward trend resulting in rapid and high gas uptake. The amount of hydrate yield is shown in Fig. 7. The hydrate yield is offered in two windows where the conversion is maximum up to 90 ml of the solution and abruptly decreases with the solution's further addition.

The hydrate conversion is maximum when the water–gas ratio is in the range of 1.16 to 4.08 (CH_4) and 2.35 to 8.25 (CO_2). As discussed, the seed crystal triggers at the liquid water interface and starts growing above the liquid level *via* creeping along the reactor's wall. The increased bed height reduces the reactor wall surface area. The hydrate forms on the cold metal parts and further grow with the increase in thickness. The heat and mass transfer are limited, and the maximum water is not channelized for the hydrate conversion, reducing the hydrate conversion. The morphological observations and the molar liquid water–gas ratio are in solid agreement with ascertained hypothesis.

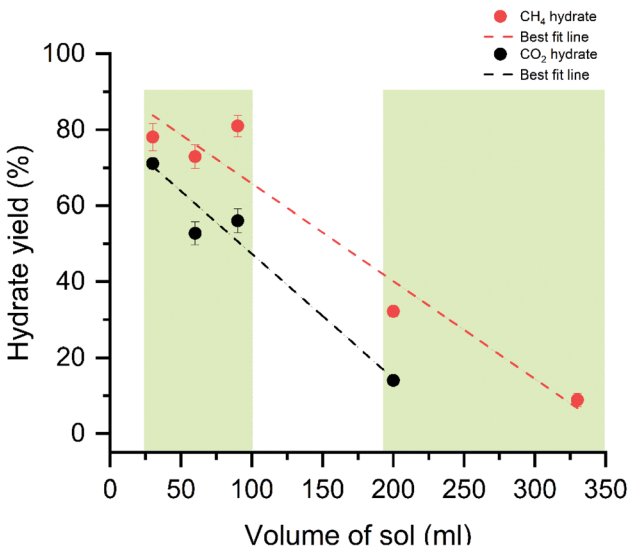

Fig. 7 The plot represents the percentage of hydrate conversion with varying solution quantities. The red and black dots represent the CH_4 and CO_2 hydrates with the standard deviation from repetitive measurements. The dashed lines are the best fit for the data points.

4. Conclusions

In summary, we have performed experiments with CH_4 and CO_2 gases in the presence of a low dose of 0.5 wt% L-methionine amino acid. The gas storage capacity and reaction time are assessed with varying solution quantities. The maximum efficiency is achieved when the molar liquid water–gas ratio is 4.08 and 8.25 for CH_4 and CO_2 hydrates. The total CH_4 and CO_2 gas storage capacity is about 14.3 ± 0.4 and 9.1 ± 0.4 liters (at STP conditions); further increasing the water–gas ratio, the gas storage capacity abruptly decreased. The molar liquid water–gas ratio strongly influences the gas storage capacity of the system. The hydrate morphology shows the hydrate creeps across the reactor's metal surface; the case is the same for CH_4 and CO_2 systems. When the hydrate fully covers the surface, the growth continues horizontally (increased thickness). With varying water–gas ratios (low to high), the formation kinetics (t_{90}) is delayed. Due to inefficient gas–water interaction, the hydrate formation rate gradually decreases with an increased water–gas ratio. The water adsorbed by the hydrate particles became interstitial, not directly contacting the gas. The gas water interaction is possible only through the diffusion process, a controlling factor for hydrate growth. Optimizing the molar liquid water–gas ratio yields high gas storage capacity and a faster CH_4 and CO_2 hydrates growth rate—the proposed methodology and the appropriate water–gas ratio help scale up the process.

Author contributions

Pinnelli S. R. Prasad: conceptualization, methodology, supervision, writing – review & editing. Burla Sai Kiran: data curation, investigation, software, validation, writing – original draft.

Conflicts of interest

There are no conflicts to declare.

Acknowledgements

The authors sincerely thank the Director of the National Geophysical Research Institute, Hyderabad, for his encouragement and permission to publish this paper (NGRI/Lib/2021/Pub-168). Partial financial support from MoES (India) and DGH-NGHP (India) are acknowledged. The first author (BSK) acknowledges the Council of Scientific and Industrial Research (CSIR) for the Senior Research Fellowship (SRF-Direct).

References

1 E. D. Sloan and C. A. Koh, *Clathrate hydrates of natural gases*, CRC Press, 2007.
2 P. Dewangan, G. Sriram, A. Kumar, A. Mazumdar, A. Peketi, V. Mahale, S. S. C. Reddy and A. Babu, *Mar. Pet. Geol.*, 2021, **124**, 104783.
3 P. Kumar, T. S. Collett, K. M. Shukla, U. S. Yadav, M. V. Lall and K. Vishwanath, *Mar. Pet. Geol.*, 2019, **108**, 3–38.
4 T. S. Collett, R. Boswell, W. F. Waite, P. Kumar, S. K. Roy, K. Chopra, S. K. Singh, Y. Yamada, N. Tenma, J. Pohlman and M. Zyrianova, *Mar. Pet. Geol.*, 2019, **108**, 39–142.
5 D. Oppo, L. De Siena and D. B. Kemp, *Sci. Rep.*, 2020, **10**, 2562.
6 I. B. Mizandrontsev, V. V. Kozlov, V. G. Ivanov, K. M. Kucher, E. S. Korneva and N. G. Granin, *Water Resour.*, 2020, **47**, 122–129.
7 A. Yatsuk, R. Shakirov, A. Gresov and A. Obzhirov, *Geo-Mar. Lett.*, 2019, **40**, 481–490.
8 A. Mazzini, M. K. Ivanov, J. Parnell, A. Stadnitskaia, B. T. Cronin, E. Poludetkina, L. Mazurenko and T. C. E. van Weering, *Mar. Geol.*, 2004, **212**, 153–181.
9 C. Sahu, R. Kumar and J. S. Sangwai, *Energy Fuels*, 2020, **34**, 11813–11839.
10 P. S. R. Prasad, B. S. Kiran and K. Sowjanya, *RSC Adv.*, 2020, **10**, 17795–17804.
11 B. Sai Kiran, K. Sowjanya, P. S. R. Prasad and J.-H. Yoon, *Oil Gas Sci. Technol.*, 2019, **74**, 12.
12 P. S. R. Prasad and B. Sai Kiran, *Sci. Rep.*, 2018, **8**, 8560.
13 B. S. Kiran and P. S. R. Prasad, *ACS Omega*, 2018, **3**, 18984–18989.
14 G. Bhattacharjee, M. N. Goh, S. E. K. Arumuganainar, Y. Zhang and P. Linga, *Energy Environ. Sci.*, 2020, **13**, 4946–4961.
15 H. P. Veluswamy, A. Kumar, R. Kumar and P. Linga, *Appl. Energy*, 2017, **188**, 190–199.
16 H. P. Veluswamy, G. Bhattacharjee, J. Liao and P. Linga, *Energy Fuels*, 2020, **34**, 15257–15269.
17 J. S. Pandey, Y. J. Daas and N. von Solms, *Processes*, 2020, **8**, 124.
18 B. S. Kiran, K. Sowjanya, V. V. Eswari and P. S. R. Prasad, *Curr. Sci.*, 2018, **114**, 661–666.
19 Q. Zhang, J. Zheng, B. Zhang and P. Linga, *Appl. Energy*, 2021, **287**, 116576.
20 S. Nallakukkala and B. Lal, *J. Environ. Chem. Eng.*, 2021, **9**, 105053.
21 P. Babu, C. Bollineni and N. Daraboina, *Energy Fuels*, 2021, **35**, 2514–2519.
22 J.-n. Zheng and M. Yang, *Desalination*, 2020, **478**, 114284.
23 A. Stoporev, R. Mendgaziev, M. Artemova, A. Semenov, A. Novikov, A. Kiiamov, D. Emelianov, T. Rodionova, R. Fakhrullin and D. Shchukin, *Appl. Clay Sci.*, 2020, **191**, 105618.
24 A. Mohammadi, *J. Mol. Liq.*, 2020, **309**, 113175.
25 Y. Liu, J. Han and H. You, *Energy*, 2020, **190**, 116201.
26 A. M. Javidani, S. Abedi-Farizhendi, A. Mohammadi, A. H. Mohammadi, H. Hassan and H. Pahlavanzadeh, *J. Mol. Liq.*, 2020, **304**, 112665.
27 C. Cheng, F. Wang, Y. Tian, X. Wu, J. Zheng, J. Zhang, L. Li, P. Yang and J. Zhao, *Renewable Sustainable Energy Rev.*, 2020, **117**, 109492.
28 J. Zheng, N. K. Loganathan, J. Zhao and P. Linga, *Appl. Energy*, 2019, **249**, 190–203.
29 T. Claßen, P. Seidl, S. Loekman, B. Gatternig, C. Rauh and A. Delgado, *Curr. Opin. Food Sci.*, 2019, **29**, 48–55.

30 E. D. Sloan, *Natural gas hydrates in flow assurance*, Gulf Professional Publishing, 2010.
31 B. S. Kiran, G. Rama Rao and P. S. R. Prasad, *Petrol. Petrochem. Eng. J.*, 2020, **4**, 000234.
32 L. Wan and D. Q. Liang, *J. Ind. Eng. Chem.*, 2021, **96**, 183–193.
33 Y. D. Zhang, X. D. Shen and N. Maeda, *Energy Fuels*, 2020, **34**, 2790–2799.
34 X. Zhang, E. O. Straume, G. A. Grasso, R. E. M. Morales and A. K. Sum, *Fuel*, 2020, **262**, 116558.
35 A. Qasim, M. S. Khan, B. Lal, M. C. Ismail and K. Rostani, *Fuel*, 2020, **259**, 116219.
36 F. O. Goodness, A. A. Sarah and A. O. Oluwatoyin, *Curr. J. Appl. Sci. Technol.*, 2020, **38**, 1–8.
37 L. Mu and N. von Solms, *J. Pet. Sci. Eng.*, 2020, **188**, 106940.
38 D. Lee, W. Go and Y. Seo, *Fuel*, 2020, **263**, 116689.
39 Y. Kim, I. I. Q. Afonso, H. Jang and J. Lee, *J. Ind. Eng. Chem.*, 2020, **82**, 349–358.
40 The editor Statistical Review of World Energy, BP p.l.c., 1St James's Square London, SW1Y 4PD UK, http://sr@bp.com.
41 In *Handbook of Liquefied Natural Gas*, ed. S. Mokhatab, J. Y. Mak, J. V. Valappil and D. A. Wood, Gulf Professional Publishing, Boston, 2014, pp. 147–183, DOI: 10.1016/B978-0-12-404585-9.00003-9.
42 In *Handbook of Natural Gas Transmission and Processing*, ed. S. Mokhatab, W. A. Poe and J. G. Speight, Gulf Professional Publishing, Burlington, 2006, pp. 295–322, DOI: 10.1016/B978-075067776-9/50013-0.
43 H. Kanda, *Economic study on natural gas transportation with natural gas hydrate (NGH) pellets*, Amsterdam, Netherlands, 2006.
44 X. Yuan, B. Zhang, R. Liang, R. Wang and Y. Sun, *Appl. Sci.*, 2020, **10**, 1701.
45 W. C. Ikealumba and H. Wu, *Energy Fuels*, 2014, **28**, 3556–3586.
46 S. Yang, D. Xu, Y. Cui, Y. Ni and C. Duan, *Nat. Resour.*, 2015, **06**, 306–311.
47 E. D. Sloan, *Nature*, 2003, **426**, 353–359.
48 Z. Zhang, T. Borhani, M. El-Naas, S. Soltani and Y. Yan, *Processes*, 2020, **8**, 70.
49 D. Saha, H. A. Grappe, A. Chakraborty and G. Orkoulas, *Chem. Rev.*, 2016, **116**, 11436–11499.
50 H. P. Veluswamy, P. Y. Lee, K. Premasinghe and P. Linga, *Ind. Eng. Chem. Res.*, 2017, **56**, 6145–6154.
51 L. Shi, J. Ding and D. Liang, *Energy*, 2019, **180**, 978–988.
52 H. Li, N. Wei, L. Jiang, J. Zhao, Z. Cui, W. Sun, L. Zhang, S. Zhou, H. Xu, X. Zhang, C. Zhang and X. Wang, *Energies*, 2020, **13**, 531.
53 J. Lee, K.-S. Kim and Y. Seo, *Chem. Eng. J.*, 2019, **375**, 121974.
54 J. Lee, Y. K. Jin and Y. Seo, *Chem. Eng. J.*, 2018, **338**, 572–578.
55 Y. Wang, D.-L. Zhong, Z. Li and J.-B. Li, *Energy*, 2020, **197**, 117209.
56 G. Yue, F.-x. Gao, Y.-w. Wang, Z. Xu, Y. Liu, Q. Sun, X.-x. Li, L.-y. Yang, A.-x. Liu and X.-q. Guo, *J. Chem. Eng. Data*, 2019, **64**, 5824–5837.
57 J. Seol, J. Park and W. Shin, *Chem. Commun.*, 2020, **56**, 8368–8371.
58 P. S. R. Prasad and V. D. Chari, *J. Nat. Gas Sci. Eng.*, 2015, **25**, 10–14.
59 V. Dhanunjana Chari, D. V. S. G. K. Sharma and P. S. R. Prasad, *Fluid Phase Equilib.*, 2012, **315**, 126–130.
60 K. Shin, Y. Kim, T. A. Strobel, P. S. Prasad, T. Sugahara, H. Lee, E. D. Sloan, A. K. Sum and C. A. Koh, *J. Phys. Chem. A*, 2009, **113**, 6415–6418.
61 P. Linga and M. A. Clarke, *Energy Fuels*, 2016, **31**, 1–13.
62 P. S. R. Prasad, Y. Sowjanya and V. Dhanunjana Chari, *J. Phys. Chem. C*, 2014, **118**, 7759–7764.
63 C. V. V. Eswari, B. Raju, V. D. Chari, P. S. R. Prasad and K. Sain, *Mar. Pet. Geol.*, 2014, **58**, 199–205.
64 V. D. Chari, P. S. R. Prasad and S. R. Murthy, *Oil Gas Sci. Technol.*, 2014, **70**, 1125–1132.
65 B. Raju, C. V. V. Eswari, V. D. Chari and P. S. R. Prasad, *Methane hydrates with nano/micro size stböer silica*, Beijing, China, 2014.
66 V. D. Chari, B. Raju, P. S. R. Prasad and D. N. Rao, *Energy Fuels*, 2013, **27**, 3679–3684.
67 Z. Liu, Y. Li, W. Wang, G. Song, Z. Lu, Y. Ning and S. Liu, *Fuel*, 2021, **293**, 120320.
68 F. Asadi, N. N. Nguyen and A. V. Nguyen, *Energy Fuels*, 2020, **34**, 9971–9977.
69 J. S. Pandey, Y. J. Daas and N. von Solms, *Processes*, 2019, **7**, 598.
70 Y. He, M.-T. Sun, C. Chen, G.-D. Zhang, K. Chao, Y. Lin and F. Wang, *J. Mater. Chem. A*, 2019, **7**, 21634–21661.
71 A. Kumar, G. Bhattacharjee, B. D. Kulkarni and R. Kumar, *Ind. Eng. Chem. Res.*, 2015, **54**, 12217–12232.
72 P. S. R. Prasad and B. S. Kiran, *Adv. Chem. Eng.*, 2020, **3**, 100022.
73 P. S. R. Prasad, B. S. Kiran and K. Sain, *Curr. Sci.*, 2018, **114**, 1163–1165.
74 P. S. R. Prasad and B. S. Kiran, *J. Nat. Gas Sci. Eng.*, 2018, **52**, 461–466.
75 Q. Nasir, H. Suleman and Y. A. Elsheikh, *J. Nat. Gas Sci. Eng.*, 2020, **76**, 103211.
76 W. F. Hao, J. Q. Wang, S. S. Fan and W. B. Hao, *Energy Convers. Manage.*, 2008, **49**, 2546–2553.
77 F. Rossi, M. Filipponi and B. Castellani, *Appl. Energy*, 2012, **99**, 167–172.
78 W. X. Pang, G. J. Chen, A. Dandekar, C. Y. Sun and C. L. Zhang, *Chem. Eng. Sci.*, 2007, **62**, 2198–2208.
79 H. P. Veluswamy, A. J. H. Wong, P. Babu, R. Kumar, S. Kulprathipanja, P. Rangsunvigit and P. Linga, *Chem. Eng. J.*, 2016, **290**, 161–173.
80 H. P. Veluswamy, S. Kumar, R. Kumar, P. Rangsunvigit and P. Linga, *Fuel*, 2016, **182**, 907–919.